Statics and Dynamics of Bidisperse Polymer Melts: A Monte Carlo Study of the Bond-Fluctuation Model

J. Baschnagel,* W. Paul, V. Tries, and K. Binder

Institut für Physik, Johannes-Gutenberg Universität, Staudinger Weg 7, D-55099 Mainz, Germany

Received December 31, 1997

ABSTRACT: As a first step toward the computer simulation of polydisperse polymeric melts, a lattice model containing two types of chains with lengths $N_1 = 20 - x$ and $N_2 = 20 + 4x$ ($0 \le x \le 10$) is studied. This variation of x, together with the fixed composition of 80% of short and 20% of long chains, leads to a polydispersity of $1 \le N_w/N_n \le 2$ (N_w, N_n: weight-, number-average chain lengths). To represent dense melts, the bond-fluctuation model at a volume fraction, $\phi = {}^1/_2$, of occupied lattice sites is used. The simulation treats both the athermal case (chain connectivity and excluded volume interaction only) and a thermal case, where additionally a choice for the bond length and bond angle potentials is made, which has recently been proposed to mimic polyethylene. For both cases number-, mass-, and z-averages of various static and dynamic quantities are calculated and compared with the results of the monodisperse melt. The main results are as follows. Whereas structural properties of the mono- and bidisperse melts agree with each other, dynamic properties are different. Short chains are slowed down by long ones, and long chains are in turn accelerated by the short species. This leads to a weaker chain length dependence of the chain's diffusion coefficient and relaxation time, which are then closer to the predictions of the Rouse theory than in the monodisperse case. For the thermal model, the stronger slowing down of the long compared to the short chains can be interpreted in terms of Arrhenius laws with an activation energy that increases with chain length.

I. Introduction

Computer simulation has become an important tool in elucidating the static and dynamic properties of polymer melts.[1−4] The simulational approach has the advantage that very detailed information on a precisely characterized model can be obtained. This implies on the one hand that many different, also experimentally inaccessible, quantities may be determined simultaneously and on the other hand that the relationship between the observed macroscopic properties and their microscopic origin can be traced. These advantages of the technique compete with the drawback that the available computational "time window" limits the range of chain lengths, N, which can be equilibrated. Whereas it is possible to work with $N \sim 10^4$ in lattice simulations of isolated self-avoiding walks,[5,6] the chain length has to be reduced by 2 orders of magnitude to allow the equilibration of a chemically realistic model for polyethylene at high temperatures, for instance.[7] Nevertheless, these simulations of short chains in the dense state are worthwhile to test basic theoretical concepts, such as the Rouse model, which underlies the reptation theory for the dynamics of high molecular weight polymers.[8]

In experimental samples there is always some polydispersity.[9−11] Contrary to that, most of the simulations deal with strictly monodisperse systems only. This simplification is justified when addressing universal properties of polymers, which are not specific to a particular material, and emerge in the limit $N \to \infty$. Recently, however, there has been increasing interest in modeling specific polymers, especially polyethylene,[7,12−24] in order to be able to compare with pertinent experimental data. In this context, it is important to assess the effects that polydispersity may have on the physical properties under consideration. Of course, many aspects of this question are also of general interest for other polymers.

While the influence on the collective scattering function,[26] the phase diagram,[27] and the unmixing kinetics[28] has been considered, for homopolymers mostly effects on the equation of state[29,30] and on the dynamics of strongly entangled melts were investigated.[31−33] To the best of our knowledge, neither the high-temperature nor the glassy dynamics of short, nonentangled polydisperse melts has found much attention.

With the present work we want to make a first step toward a modeling of such a situation by considering the simplest case of polydispersity, a bidisperse mixture. Though being very distinct from the typical molecular weight distributions of polymerization reactions,[10,11] bidisperse systems were analyzed in many of the above-mentioned theoretical studies[26,30−33] and in a recent neutron-scattering experiment on saturated polybutadiene.[34] In our simulations we fixed the number-average chain length, N_n, at a value which is smaller than the entanglement length and varied the polydispersity index N_w/N_n (N_w: weight-average chain length) from 1 (monodisperse) to 2 (moderately polydisperse). By comparing the results of the mono- and the polydisperse melts, we want to find out to what extent the static and dynamic properties of a chain with a specific length differ in the pure and composed systems.

The remainder of the paper is organized as follows: In section II we introduce the bond-fluctuation model, the simulation parameters and the pertinent averages over the chain length distribution. Section III discusses polydispersity effects in the framework of the Rouse model and derives the theoretical predictions for the simulated quantities. The result section, section IV, is split into two parts. Part IVA deals with properties of

* To whom correspondence should be addressed. E-mail: baschnag@flory.physik.uni-mainz.de.

S0024-9297(97)01886-X CCC: $15.00
Published on Web 05/23/1998

Table 1. Parameters of the Effective Potentials in Eqs 6 and 7

u_0	u_1	l_0	l_1	v_0	v_1	c_0	c_1
282.828613	−4.818017	3.271217	5.752445	581.588379	−0.486899	−0.671640	21.517746

[a] Note that l_0, l_1 are given in units of the lattice spacing, u_0, u_1, v_0, v_1 are given in units of degree Kelvin, while c_0 and c_1 are dimensionless.

a purely athermal melt, whereas part IVB presents the results for a model of polyethylene in a temperature interval ranging from the high-temperature to the strongly supercooled state. The final section, section V, contains our conclusions.

II. Model and Chain Length Averages

A. Athermal and Thermal Bond-Fluctuation Model and the Random Hopping Algorithm: A Lattice Model for Polymer Melts with Rouse Dynamics. All simulations were performed with the bond-fluctutation model which is described in detail in refs 35−38. The motion of the monomers is generated by the Monte Carlo technique: A monomer and a lattice direction are chosen at random, and a move is attempted in the proposed direction. The move is successful, if the targeted sites are empty (excluded volume interaction) and if it lowers the energy. On the other hand, if the energy difference, ΔE, between the final and the initial state is positive, the move is only accepted with probability $\exp[-\Delta E/T]$,[1,25] where T denotes the temperature (Boltzmann constant $k_B = 1$). By means of this probability, temperature is introduced into the simulation. Athermal conditions correspond to a situation where the temperature is so high that the exponential function is always 1 and the dynamics is exclusively determined by the excluded volume interaction. After all monomers in the systems have obtained the chance to move once, one time step of the Monte Carlo simulation, the Monte Carlo step (MCS), is complete. *A priori*, this "pseudo-time" has no relation to the physical time scale. However, it is possible to translate the lattice constant into angstroms and the MCS into seconds when simulating real materials, such as polyethylene (see below).

The just described "random-hopping" dynamics is supposed to mimic a random force that a monomer experiences due to collisions with its neighbors. It leads to Rouse-like dynamics,[8,39] as the following scaling argument shows. The random force tries to move a monomer over a distance of the effective bond length b ($b = (C_\infty\langle l^2\rangle)^{1/2}$; C_∞, characteristic ratio for $N \to \infty$; $\langle l^2\rangle$, mean-square bond length). This local displacement entails a motion of order b/N for the center of mass. However, the collisions with surrounding monomers impede the motion. The combined effect is that a monomer has a (temperature, density, etc. dependent) mobility, W, which determines the acceptance rate of a move. To displace the center of mass by b in one time unit, $W \times N$ such random motions are needed. This implies that the mean-square displacement of the center of mass scales as ($\boldsymbol{r}_{cm}(t)$: position vector of the center of mass at time t)

$$g_3(t) = \langle[\boldsymbol{r}_{cm}(t) - \boldsymbol{r}_{cm}(0)]^2\rangle \sim WN(b/N)^2 t \qquad (1)$$

Since the center of mass moves due to the addition of random displacements, it exhibits a free diffusive behavior

$$g_3(t) = 6D_N t \qquad (2)$$

A comparison of eqs 1 and 2 yields the Rouse result for the diffusion coefficient

$$D_N \sim \frac{Wb^2}{N} \qquad (3)$$

Arguing furthermore that a chain has relaxed when its center of mass has diffused over the distance of the radius of gyration, R_g, the relaxation time, τ_N, is given by

$$g_3(\tau_N) \sim (Wb^2/N)\tau_N \stackrel{!}{=} R_g{}^2 \sim b^2 N \qquad (4)$$

so that

$$\tau_N \sim \frac{N^2}{W} \qquad (5)$$

which scales as the Rouse time. These scaling arguments assume that there are no hydrodynamic interactions, that the excluded volume interaction is screened down to the length scale of a bond, and that entanglements are not effective yet. The first condition is satisfied, since the model does not contain solvent molecules, the second can be met by simulating at a volume fraction, ϕ, of occupied lattice sites of $\phi = 0.5$, and the third by choosing the longest chains in the (bidisperse) melt not much larger than the entanglement chain length $N_e \approx 30$.[37,38]

In previous work,[23,40,41] a "mapping" procedure was developed to augment the athermal bond-fluctuation model by temperature dependent potentials, $U(l)$ and $U(\theta)$, for the bond length, l, and the bond angle, θ. These potentials are constructed such that both the chain radii of polyethylene chains in the melt and the local mobility of the monomers are reproduced over a wide range of temperatures.[23,40]

$$U(l) = \Phi_0 u_0 (l - l_0)^2 + \Phi_1 u_1 (l - l_1)^2 \qquad (6)$$

$$U(\theta) = \Phi_0 v_0 (\cos\theta - c_0)^2 + \Phi_1 v_1 (\cos\theta - c_1)^2 \qquad (7)$$

Here $\Phi_0 = 1$ and $\Phi_1 = (1/T - \langle 1/T\rangle)/(\langle 1/T^2\rangle - \langle 1/T\rangle^2)^{1/2}$ (with $\langle 1/T\rangle = (\Sigma_{i=1}^{k}\, 1/T_i)/k$) are orthonormal basis functions on the set of temperatures $\{T_i\}$, where input information for the mapping is given, while the parameters u_0, u_1, l_0, l_1, v_0, v_1, c_0 and c_1 are fitted by a nonlinear optimization procedure, as described by Tries *et al.*[23] The values of these parameters are given in Table 1.

By this mapping procedure, $n = 5$ successive CH_2-units are mapped onto one effective bond of the bond-fluctuation model. When the density is matched at $T = 509$ K—where many experimental data were available for comparison—with the experimental density, the scale factor, s, to convert the lattice constant into physical units, is given by $s = 2.034$ Å. Using furthermore the fact that the configurational changes of polyethylene coils come about by (trans ↔ gauche$^+$, gauche$^-$) jumps over a rather high barrier (≈1500 K) in the torsional potential, it is possible to detemine an effective time

scaling factor that translates a MCS into the physical time,[23]

$$t_{\text{scale}} = 1.22 \times 10^{-3} \exp\left(\frac{1418\ \text{K}}{T}\right)\left[\frac{\text{ps}}{\text{MCS}}\right] \qquad (8)$$

B. Bidisperse and Polydisperse Melts: Static Averages over the Molecular Weight Distribution. To simulate a bidisperse melt we compose the system of a large number ($P_1 = 160$) of short chains (species 1) and a small number ($P_2 = 40$) of long chains (species 2). In total there are $P = P_1 + P_2 = 200$ chains. The chain lengths of the short and the long species are taken as $N_1 = 20 - x$ and $N_2 = 20 + 4x$ with $x = 0, 1, ..., 10$. The lower bound, $x = 0$, corresponds to the monodisperse melt, and the upper bound, $x = 10$, leads to a chain length disparity of $N_1 = 10$ and $N_2 = 60$. This bound was imposed because the 20% of long chains exceed $N_e = 30$ only by a factor of 2—thus entanglement effects should be negligible in our simulation.

The values, $P_1 = 160$ and $P_2 = 40$, imply that the probability (number fraction) for a short or a long chain is $p_1 = 0.8$ or $p_2 = 0.2$, respectively. This asymmetric distribution with the higher weight for the short chains was chosen because it represents the bidisperse counterpart of realistic molecular weight distributions, as they result from step polymerizations (Schulz−Flory distribution), for instance.[10,11] By virtue of p_1 and p_2 the probability to find a chain of (arbitrary) length N is given by

$$p_N = p_1\delta_{N,N_1} + (1 - p_1)\delta_{N,N_2}, \quad \sum_{N=1}^{\infty} p_N = 1 \qquad (9)$$

This probability serves to introduce the following averages. Let $A(N)$ be an observable which depends on N. Then one can define the "number-", "weight-", and "z-average" as

$$[A(N)]_n = \sum_{N=1}^{\infty} p_N A(N),$$

$$[A(N)]_w = \frac{\sum_{N=1}^{\infty} (p_N N) A(N)}{\sum_{N=1}^{\infty} p_N N}, \quad [A(N)]_z = \frac{\sum_{N=1}^{\infty} (p_N N^2) A(N)}{\sum_{N=1}^{\infty} p_N N^2} \qquad (10)$$

Equation 10 holds for any molecular weight distribution p_N. The specified averages are often measured in experiments.

The first two averages have an intuitive interpretation. In the number-average one counts the chains with length N, multiplies the result, P_N, with $A(N)$, and divides by the total number of chains (*i.e.*, by $\sum_N P_N = P$). On the other hand, in the weight-average one weighs the chains of length N and divides by the total weight, $\sum_N P_N N$, of the melt.

As an example, let $A(N)$ be the chain length N. Then eq 10 yields the number-average, weight-average, and z-average chain lengths

$$N_n := [N]_n = \sum_{N=1}^{\infty} p_N N, \quad N_w := [N]_w = \frac{[N^2]_n}{[N]_n},$$

$$N_z := [N]_z = \frac{[N^3]_n}{[N^2]_n} \qquad (11)$$

The number-average, N_n, can be measured by colligative methods, such as membrane osmometry or boiling point elevation, the weight-average, N_w, is the typical average obtained in light or neutron scattering experiments, and the z-average, N_z, can be determined by ultracentrifugation techniques.[11]

In a polydisperse melt it is not sufficient to focus on one particular average. For instance, specifying only N_n could be very misleading because many polymeric properties are not determined by the number, but by the mass of the chains. However, the dominant contribution to N_n comes from the light particles. To see this, let w_N denote the weight fraction, $P_N N/\sum_N P_N N$, of chain length N. Using eq 11, we can write N_n and N_w as

$$N_n = \frac{1}{\sum_{N=1}^{\infty} w_N/N}, \quad N_w = \sum_{N=1}^{\infty} w_N N \qquad (12)$$

This shows that N_n is dominated by a small weight fraction of light chains, whereas the main contribution to N_w results from a large fraction of heavy polymers. In practice, the weight-average is therefore a much better indicator of the system's properties than the number-average. The number-average mainly serves to characterize the variance of the chain length distribution because

$$\frac{[(N - N_n)^2]_n}{N_n^2} = \frac{N_w}{N_n} - 1 \qquad (13)$$

The ratio, N_w/N_n, is called the "polydispersity index" (sometimes the right-hand side of eq 13 is abbreviated by U and called the "polydispersity coefficient"[10] or the "non-uniformity"[42]). Equation 13 shows that N_n is in general smaller than N_w, which in turn is smaller than N_z.

Up to now, the discussion, presented in eqs 10−13, referred to a general distribution of chain lengths. If we insert eq 9 into eq 11, we obtain the specific results for the bidisperse mixture, *i.e.*,

$$N_n = 20, \quad N_w = N_n\left[1 + \frac{x^2}{100}\right],$$

$$N_z = N_n\left[\frac{1 + 3x^2/100 + 3x^3/2000}{1 + x^2/100}\right] \qquad (14)$$

When using the lower and upper bounds for x ($x = 0$, 10), eq 14 yields

$$1 \le \frac{N_w}{N_n} \le 2, \quad 1 \le \frac{N_z}{N_w} \le 1.375 \qquad (15)$$

The range of these variations is physically reasonable,

as a comparison with experimental data[43−46] and with the predictions of the Schulz−Flory distribution[11] shows.

III. Polydispersity and the Rouse Model

In the Rouse model[8,39] a chain of N effective monomers (Brownian beads), connected by harmonic springs, is exposed to a medium which exerts friction (and random uncorrelated forces) on the beads of the chain. It is believed that the dynamics of the polymers in a melt of short (nonentangled) chains decouples so that the environment of a considered chain can simply be considered as a thermal heat bath described by the Rouse model. Evidence for this assumption comes from both experiments[46,47] and simulations.[3,48]

Since the Rouse model neglects excluded volume interactions, the chains obey Gaussian statistics, *i.e.*, the (mean-square) end-to-end distance, R^2, and the radius of gyration, R_g^2, scale as $R^2 = b^2N$ and $R_g^2 = b^2N/6$. Due to the linear dependence on N the number-, weight-, and z-averages of R^2 and R_g^2 in a polydisperse melt are directly proportional to the respective chain length averages. For example, the z-average of R_g^2 is

$$R_{g,z}{}^2 := [R_g{}^2(N)]_z = \frac{1}{6}b^2N_z \simeq \frac{1}{6}b^2N_w \qquad (16)$$

where the latter approximate equality holds for weakly polydisperse systems (see eq 15).

Both $R_{g,z}{}^2$ and N_w can be determined in light or neutron scattering experiments by measuring the collective structure factor of a chain in the melt. In a dense melt the structure factor, $S_N(q)$, of a chain of length N is very well described by the Debye function $f(x)$ (for $q \leq 2\pi/b$)[8]

$$S_N(q) = \frac{1}{N}\sum_{n,m=1}^{N}\langle \exp(i\boldsymbol{q}\cdot[\boldsymbol{r}_n - \boldsymbol{r}_m])\rangle = Nf(q^2R_g{}^2) \qquad (17)$$

In Eq. (17) $\langle\cdot\rangle$ represents the thermal average, $\boldsymbol{q}$ is the wave vector, and $\boldsymbol{r}_n$ denotes the position vector to the nth monomer. Since the amplitude of the scattered radiation is proportional to the size of the particles, it is not the number- but the weight-average of $S_N(q)$, which is measured in a polydisperse sample, *i.e.*

$$S_w(q) := [S_N(q)]_w = [Nf(q^2R_g{}^2)]_w = N_w[f(q^2R_g{}^2)]_z \xrightarrow{qR_g \ll 1} N_w\left[1 - \tfrac{1}{3}q^2R_{g,z}{}^2\right] \qquad (18)$$

For low q values one can therefore simultaneously determine N_w and $R_{g,z}$.[49]

In addition to static properties one can also measure dynamic quantities, such as the coherent intermediate scattering function of a chain

$$S_N(q,t) = \frac{1}{N}\sum_{n,m=1}^{N}\langle \exp(i\boldsymbol{q}\cdot[\boldsymbol{r}_n(t) - \boldsymbol{r}_m(0)])\rangle \qquad (19)$$

or the incoherent intermediate scattering function

$$S_N^{inc}(q,t) = \frac{1}{N}\sum_{n=1}^{N}\langle \exp(i\boldsymbol{q}\cdot[\boldsymbol{r}_n(t) - \boldsymbol{r}_n(0)])\rangle \qquad (20)$$

where $\boldsymbol{r}_n(t)$ is the position of the nth monomer at time t. In the Rouse model the difference, $\boldsymbol{r}_n(t) - \boldsymbol{r}_m(0)$, may be expressed as a linear combination of the random force. Since the force is assumed to be Gaussian, the differences of the monomer positions are also distributed according to a Gaussian distribution. Therefore

$$S_N(q,t) = \frac{1}{N}\sum_{n,m=1}^{N}\exp\left[-\frac{1}{6}q^2\langle[\boldsymbol{r}_n(t) - \boldsymbol{r}_m(0)]^2\rangle\right] \qquad (21)$$

$$S_N^{inc}(q,t) = \frac{1}{N}\sum_{n=1}^{N}\exp\left[-\frac{1}{6}q^2\langle[\boldsymbol{r}_n(t) - \boldsymbol{r}_n(0)]^2\rangle\right] \qquad (22)$$

A special case is interesting for the following discussion. If $qR_g \ll 1$

$$\langle[\boldsymbol{r}_n(t) - \boldsymbol{r}_m(0)]^2\rangle \simeq g_3(t) = 6D_Nt \quad \text{with} \quad D_N = \frac{k_BT}{N\zeta} \qquad (23)$$

so that

$$S_N^{inc}(q,t) \simeq \frac{1}{N}S_N(q,t) \simeq \frac{S_N(q,t)}{S_N(q)} \simeq \exp[-D_Nq^2t] \qquad (24)$$

Equation 24 suggests that the diffusion coefficient be estimated either from the initial slope (so-called "first cumulant") of, e.g., $S_N^{inc}(q,t)$, or from the integral of the scattering function, *i.e.*

$$D_{slope} = -\frac{1}{q^2}\frac{d}{dt}S_N^{inc}(q,t)|_{t=0} = D_N, \qquad D_{int} = [q^2\int_0^\infty S_N^{inc}(q,t)\,dt]^{-1} = D_N \qquad (25)$$

For a monodisperse melt, both methods are identical, and it does not matter whether the coherent or the incoherent scattering function is used, provided that $qR_g \ll 1$. This changes for polydisperse melts. As discussed above, scattering experiments measure weight-averages. Using eq 10 the coherent and incoherent scattering functions are generalized in the following way

$$S_w(q,t) := [S_N(q,t)]_w = \frac{1}{N_n}\sum_{N=1}^{\infty}p_NNS_N(q,t) \xrightarrow{qR_g \ll 1} \frac{1}{N_n}\sum_{N=1}^{\infty}p_NN^2e^{-D_Nq^2t} \qquad (26)$$

$$S_w^{inc}(q,t) := [S_N^{inc}(q,t)]_w = \frac{1}{N_n}\sum_{N=1}^{\infty}p_NNS_N^{inc}(q,t) \xrightarrow{qR_g \ll 1} \frac{1}{N_n}\sum_{N=1}^{\infty}p_NNe^{-D_Nq^2t} \qquad (27)$$

These equations show that polydispersity leads to a true broadening of the relaxation spectrum: quantities, which exhibit a single exponential decay, such as eq 24, now decay with a distribution of relaxation times.

When the diffusion coefficient is determined from Eq. 25, one obtains

$$D_{\text{slope}}^{\text{coh}} = -\frac{1}{q^2 N_w}\frac{d}{dt}S_w(q,t)\Big|_{t=0} = \frac{k_B T}{N_w \zeta},$$

$$D_{\text{int}}^{\text{coh}} = \left[\frac{q^2}{N_w}\int_0^\infty [e^{-D_N q^2 t}]_w \, dt\right]^{-1} = \frac{k_B T}{N_z \zeta} \quad (28)$$

from coherent scattering, and

$$D_{\text{slope}}^{\text{inc}} = -\frac{1}{q^2}\frac{d}{dt}S_w^{\text{inc}}(q,t)\Big|_{t=0} = \frac{k_B T}{N_n \zeta},$$

$$D_{\text{int}}^{\text{inc}}[q^2\int_0^\infty [e^{-D_N q^2 t}]_w \, dt]^{-1} = \frac{k_B T}{N_w \zeta} \quad (29)$$

from incoherent scattering. Note that the chain length dependence of the various means to calculate the diffusion coefficient is different. Since N_w is rather close to N_z for weakly polydisperse melts, the first cumulant and the integral essentially yield the same diffusion coefficient for coherent scattering. However, for incoherent scattering the difference in the chain length dependence is more pronounced and should be observable.

IV. Properties of a Bidisperse Melt

This result section is divided into two parts: In subsection IVA we compare static and dynamic properties of the bidisperse melt with those of the monodisperse system under athermal conditions ($T = \infty$). On the other hand, subsection IVB describes the corresponding results for the thermal version of the model using potentials that are tailored to approximately match the behavior of polyethylene. The temperature range studied covers the high-temperature, normal liquid and the strongly supercooled, glassy state of the melt.

A. The Athermal Case. A melt that contains a small concentration of very long chains, while all other chains are much shorter, exhibits a swelling of the long species, since the short chains act like a good solvent.[51] In our simulations we wanted to avoid such an extreme situation. Therefore it is important to establish that the choice of parameters for our model leads to ideal Gaussian statistics.

An advantage of the simulation is that averages can be calculated for each fraction, p_N, of chains with length N individually, and that the results can be compared with those of precisely the same model in the monodisperse case. Figure 1 shows such a comparison for the end-to-end distance, R^2, and the radius of gyration, R_g^2. Apparently, the change of "environment" in the bidisperse systems has a negligible effect on the chain radii. The results of the monodisperse and the bidisperse systems fall right on top of each other. In particular, there is no tendency of the longer chains to exhibit a swollen ($R^2 \sim R_g^2 \sim N^{2\nu}$ with $\nu \approx 0.59$) rather than an ideal ($\nu_{id} = 0.5$) behavior. Theoretically, this result is reasonable because a single long chain is only swollen, if $N_1 < N_2^{1/2}$.[51] Since we have $N_1 > N_2^{1/2}$, even for $x = 10$, and the volume fraction of the long species is above the overlap concentration, swelling is not expected.

However, this ideal behavior is not borne out for all chain lengths studied. For small N the log−log plot (Figure 1) exhibits a slightly steeper slope, indicating

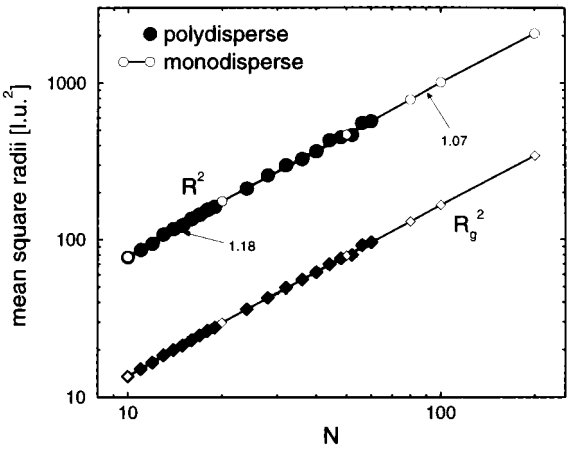

Figure 1. Mean-square end-to-end distance, R^2, (upper curve) and radius of gyration, R_g^2, (lower curve) on a log-log plot vs chain length, N, for the bond-fluctuation model on the simple cubic lattice. We chose a $L \times L \times L$ lattice with $L = 40$ and periodic boundary conditions. The volume fraction of occupied lattice sites is $\phi = 0.5$ (for a detailed description of the model, see ref 37, from which the data for the monodisperse melts (open symbols) were taken). The filled symbols represent the simulation results for the chains of length N in the bidisperse melt. The thermal averages in this case are based on runs, extending over 10^7 attempted moves per monomer, and on seven statistically independent replicas of the the start configurations for the runs. Note that all lengths are measured in units of the lattice spacing [l.u.]. Numbers at the upper curve denote effective exponents (slopes of straight line fits).

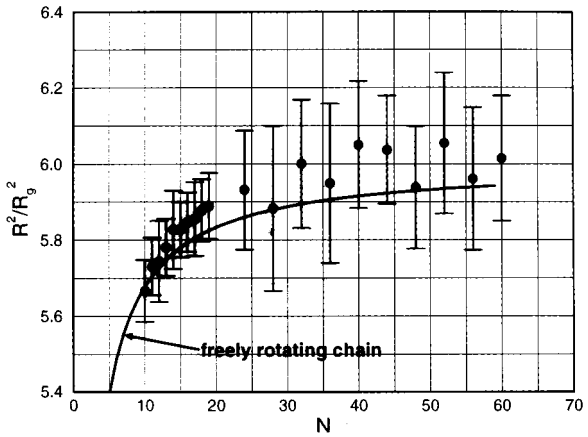

Figure 2. Plot of R^2/R_g^2 vs N for the bidisperse mixture having 80% of short chains with length $N_1 = 20 - x$ and 20% of long chains with length $N_2 = 20 + 4x$. The model parameter x, which controls the polydispersity, ranges from $x = 0$ to $x = 10$ (see section II for details). The solid curve is the result for the freely rotating chain (see eq 30).

an "effective exponent" $\nu_{\text{eff}} > \nu_{\text{id}}$. The reason for this deviation is that R_g becomes comparable to the screening length for the excluded volume interaction if N is too small.[37]

To check for which chain lengths the deviation from Gaussian statistics becomes negligible, Figure 2 presents a plot of R^2/R_g^2 vs N. For ideal Gaussian chains this ratio is 6. The figure shows that this value is reproduced within statistical error for $N \geq 25$, while systematic deviations clearly occur for smaller N. However, these deviations are quite similar to those of a freely rotating chain.[53] This is a chain model, in which the bond length and bond angle are fixed and each bond is allowed to rotate freely around the direction of the preceding bond. Therefore the excluded volume interaction is only accounted for locally between three

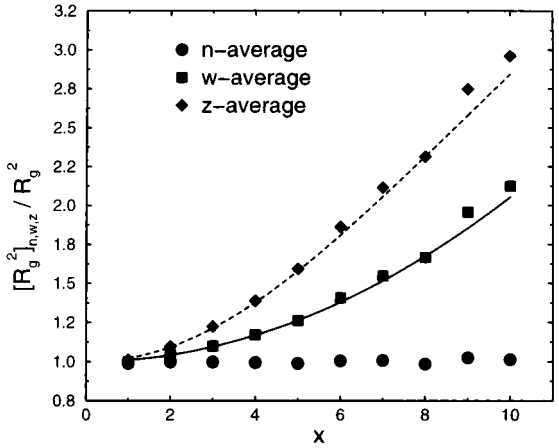

Figure 3. Number- (circles), weight- (squares), and *z*-averaged (diamonds) radius of gyration vs the polydispersity parameter *x*. The respective averages of the gyration radius, $[R_g^2]_{n,w,z}$, are divided by the monodisperse value for $N = 20$, *i.e.*, by $R_g^2 = 29.7$.[37] The solid and broken curves are the theoretical expectations for random walk behavior, eq 31.

sucessive monomers (trimer approximation) but neglected for larger distances along the backbone of the chain. For our application we used a variant of this model, in which the fixed bond length and angle are replaced by their averages from the simulation. This yields

$$\frac{R^2}{R_g^2} = \left[\frac{\langle l^2\rangle - \langle l\rangle^2}{\langle l^2\rangle} + \frac{1-\alpha}{1+\alpha} + \frac{2\alpha(1-(-\alpha)^{N-1})}{(N-1)(1+\alpha)^2}\right] \Bigg/ \left[\frac{N+1}{6N}\left[\frac{\langle l^2\rangle - \langle l\rangle^2}{\langle l^2\rangle} + \frac{1-\alpha}{1+\alpha}\right] + \frac{\alpha}{N(1+\alpha)^2} + \frac{2\alpha^2}{N^2(1+\alpha)^3} + \frac{2\alpha^3(1-(-\alpha)^{N-1})}{(N-1)N^2(1+\alpha)^4}\right] \quad (30)$$

where $\langle l\rangle$ (=2.604), $\langle l^2\rangle$ (=6.947), and $\alpha = \langle\cos\theta\rangle$ (= −0.1055) are the mean bond length, the mean-square bond length, and the mean cosine of the bond angle, respectively. The good agreement between the simulation data and eq 30 suggests that excluded volume forces are not relevant beyond the length scale of a trimer. This compares very well with the estimate for the screening length (about six lattice spacings) of the bond-fluctuation model at the volume fraction considered.[37]

The fact that our static results are slightly affected by deviations from the asymptotic Gaussian behavior for small N must be remembered when considering averages over the chain length distribution. In the theoretical part of section II the asymptotic behavior was assumed throughout. Nevertheless, Figure 3 illustrates that the results for the chain radii closely approximate the asymptotic expectations: $R_{g,n}^2$ is independent of x, whereas $R_{g,w}^2$ and $R_{g,z}^2$ increase with x. The solid and the dashed lines in the figure are the predictions of eq 14 when the number of bonds, $N - 1$, instead of the chain length is used, *i.e.*

$$\frac{R_{g,w}^2}{R_g^2} = 1 + \frac{x^2}{95}, \quad \frac{R_{g,z}^2}{R_g^2} = \frac{1 + 59x^2/1900 + 3x^3/1900}{1 + x^2/100} \quad (31)$$

where R_g^2 (= 29.7) is the radius of gyration of the monodisperse system.[37] Whereas the difference between $N - 1$ and N is completely negligible for asymptotically long chains, it is small, but noticable, in our case. Therefore we used eq 31 instead of eq 14 for the comparison. The figure shows that the simulation data for $R_{g,w}^2$ and $R_{g,z}^2$ gradually deviate from eq 31 with increasing x. These deviations may again be attributed to the nonideal behavior of the short chains, and are more pronounced for the *z*-average than for the weight-average moiety because a stronger N-dependence amplifies the effect.

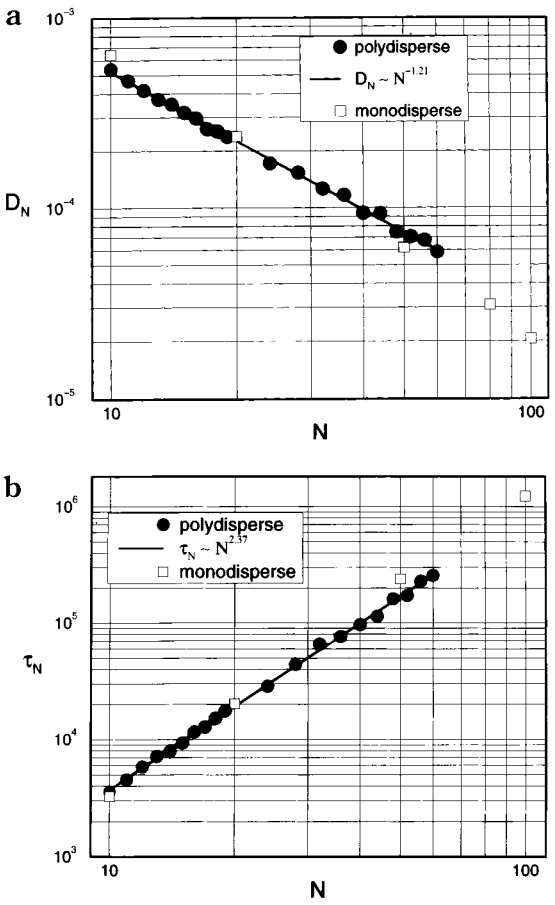

Figure 4. Log-log plot of the self-diffusion coefficient D_N (a) and the chain relaxation time τ_N (b) vs chain length N. The filled circles represent the results from the bidisperse mixtures, whereas the open squares are the simulation data for the monodisperse systems taken from refs 37 and 58. Straight lines indicate power law fits with exponents, as specified in the figures.

The dynamic properties of the bidisperse melt are exemplified in Figures 4 and 5. Parts a and b of Figure 4 compare the diffusion coefficient, D_N, and the relaxation time, τ_N, both averaged over all chains of length N in the bidisperse melt, with the corresponding results of the monodisperse system. The diffusion coefficient was calculated from the long time limit of $g_3(t)$ (see eq 2), whereas τ_N was determined by the condition $g_3(\tau_N) = R_g^2$. According to eq 4, τ_N should be proportional to the Rouse time τ_R. The figures reveal that both quantities are rather well described by power laws. However, the observed exponents are about 20% off the predicted values: $D_N \sim N^{-1.21}$ and $\tau_N \sim N^{2.37}$ instead of $D_N \sim N^{-1}$ and $\tau_N \sim N^2$. This behavior indicates that the Rouse model is not strictly valid for our bidisperse system of short, nonentangled chains. This observation has already been made in various related studies with monodisperse lattice and off-lattice models.[3,54]

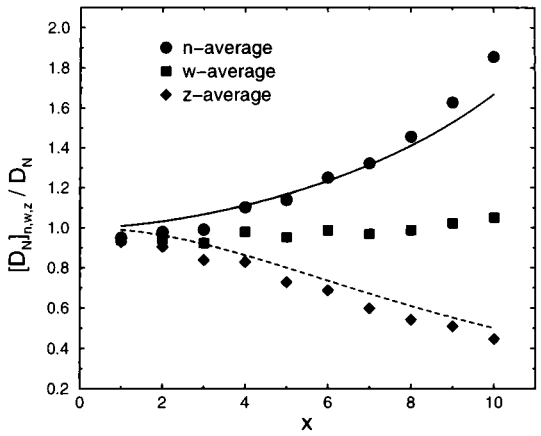

Figure 5. Number- (circles), weight- (squares), and *z*-averaged (diamonds) diffusion coefficient vs the polydispersity parameter *x*. The respective averages of the diffusion coefficient, $[D_N]_{n,w,z}$, are divided by the monodisperse value for $N = 20$, *i.e.*, by $D_N = 2.38 \times 10^{-4}$.[58] The broken and solid curves are the theoretical expectations for Rouse behavior, eqs 28 (*i.e.*, D_{slope}^{coh}) and 32.

If one tried to save the Rouse description by generalizing the friction constant to an *N*-dependent friction coefficient, $\zeta(N)$, one would also need to allow an additional dependence on the composition of the surrounding matrix, in which the chain moves. This assertion is corroborated by the chain length dependences of the mono- and bidisperse melts. A long chain in the bidisperse melt is mostly surrounded by short chains and thus experiences less friction than in the monodisperse system. On the other hand, a short chain close to a long one feels a stronger resistance against its motion. Although the static properties of the mono- and bidisperse melts coincide, there is a difference in the dynamic properties. Short and long chains mutually accelerate or slow down each other so that the *N*-dependence of D_N or τ_N is weaker and thus closer to the Rouse prediction than in the monodisperse case. At this point, it is interesting to note that "matrix effects" on friction coefficients have been nicely demonstrated by molecular dynamics simulation for a model polymer mixture, where the constituents differ only by their monomer masses.[55]

Due to these deviations from the Rouse behavior one can also expect that the predictions, eqs 28 and 29, for the bidisperse melt are not fully satisfied. Figure 5 shows the variation of the number-, weight- and *z*-averaged diffusion coefficients with the polydispersity parameter *x*. Since we calculated the pertinent averages for D_N (and not for its inverse), the simulation results correspond to the first cumulant method (see eq 25). According to eqs 26−29, the method yields the *z*-average of D_N for coherent and the weight-average for incoherent scattering. If Rouse dynamics applied, the weight-average should not depend on *x*, whereas the *z*-average should scale as N_w^{-1}. Figure 5 shows that this is approximately true. Nevertheless, one observes a slight, but systematic increase of $[D_N]_w$ with *x*, indicating that the short chains, which diffuse faster, dominate the average for large polydispersity. This increase is much more pronounced for the number-averaged diffusion coefficient because

$$[D_N]_n = \frac{k_B T}{\zeta}\left[\frac{1}{N}\right]_n = \frac{k_B T}{20\zeta}\left[\frac{4}{5 - x/4} + \frac{1}{5 + x}\right] \quad (32)$$

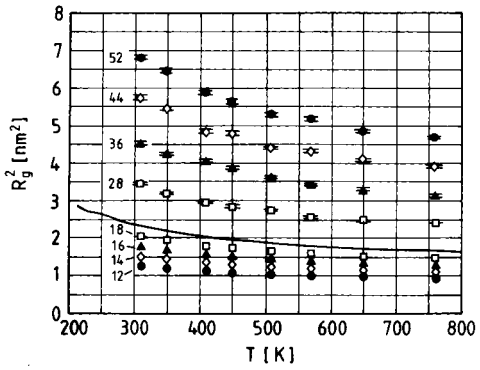

Figure 6. Radius of gyration, R_g^2, plotted vs temperature for the bond-fluctuation model with potentials adapted to mimic polyethylene.[23] Numbers represent the chain lengths, *N*, of the model (the corresponding degrees of polymerization, N_p, are obtained by multiplication with $n = 5$). Note that two chain lengths, represented by the same symbol, were simultaneously determined in one simulation of a bidisperse melt with a given polydispersity *x*. For instance, $N = 18$, 28 correspond to $x = 2$; see eq 14. Error bars are only shown for $N \geq 28$. For shorter chains they are always smaller than the symbol size. The full line are the results for the monodisperse melt with $N = 20$.

If *x* varies from $x = 0$ to $x = 10$, one expects an increase from the monodisperse result, D_N, to $5D_N/3$. The figure shows that this expectation is approximately borne out.

B. The Thermal Case: Polyethylene as an Example. In order to exemplify the thermal behavior of our model this section describes the simulation results for the case, where appropriate bond length and bond angle potentials were introduced to mimic the large length and time scale properties of polyethylene.[23] Such a "mapping" procedure allows a translation of the abstract Monte Carlo units to physical units: a lattice constant corresponds to 2.034 Å, the Monte Carlo time step is related by eq 8 to seconds, and one monomer of the bond-fluctuation model represents a group of $n = 5$ CH_2 units. Therefore the studied range of chain lengths, $N = 10-60$, corresponds to a degree of polymerization of $N_p = nN = 50-300$. While the following figures thus contain physical units for the lengths and temperatures, we have kept the chain lengths, *N*, of the coarse-grained model and sometimes also the time in MCS's to facilitate the comparison with the results of the preceding section.

Figure 6 shows the temperature dependence of the radius of gyration, calculated from bidisperse mixtures with $x = 2$, 4, 6, and 8. Note that there are always pairs of chain lengths, denoted by the same symbol, which represent the simulation results of one mixture with a specific *x* value (for instance, $N = 18$ and $N = 28$ correspond to $x = 2$). As in the monodisperse case the radii gradually increase with decreasing temperature, reflecting the tendency of the chains to expand. This expansion slightly depends on chain length. For instance, the radius of gyration for $x = 2$ ($N_w/N_n = 1.04$) increases by a factor of about 1.35 for both chain lengths in the considered temperature interval. This is consistent with the monodisperse behavior. On the other hand, for $x = 8$ ($N_w/N_n = 1.64$) the short chains ($N = 12$) expand by a factor of 1.3, but the long species expands by about 1.4. Nevertheless, these differences are so weak that the behavior observed at infinite temperature is essentially recovered. Within the statistical uncertainties there are only minor deviations between the number-averaged radii of gyration and the monodisperse results (Figure 7a), whereas the weight-

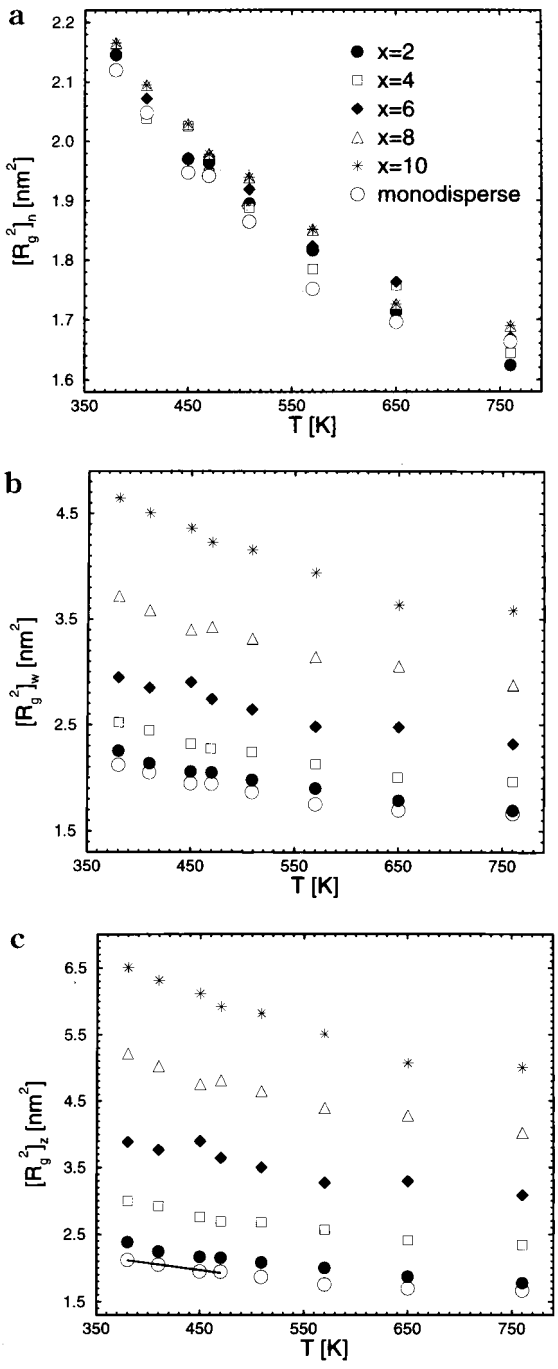

Figure 7. Comparison of the number-averaged, $[R_g^2]_n$, (a), weight-averaged, $[R_g^2]_w$, (b) and z-averaged, $[R_g^2]_z$, (c) radius of gyration with the monodisperse result for $N = 20$. The model is the same as in Figure 6. The various symbols denote different polydispersities, x, as specified in panel a. The x -values correspond to $N_w/N_n = 1.04$ ($x = 2$), $N_w/N_n = 1.16$ ($x = 4$), $N_w/N_n = 1.36$ ($x = 6$), $N_w/N_n = 1.64$ ($x = 8$), and $N_w/N_n = 2$ ($x = 10$). For $[R_g^2]_z$ a solid line is additionally shown for the monodisperse data. It represents a fit to the linear form $([R_g^2]_z)^{1/2} = aT + b$, which is motivated by the experimental analysis of ref 56. The results of the fit are $a \approx -7.4 \times 10^{-4}$ nm/K and $b \approx 1.73$ nm.

and the z-averages exhibit a strong enhancement with increasing polydispersity (see parts b and c of Figure 7). However, as at $T = \infty$ (Figure 3) the enhancement follows eq 14 rather closely (see Figure 8). This indicates that the chains are sufficiently long to preserve the (almost) Gaussian structure in the studied temperature interval.

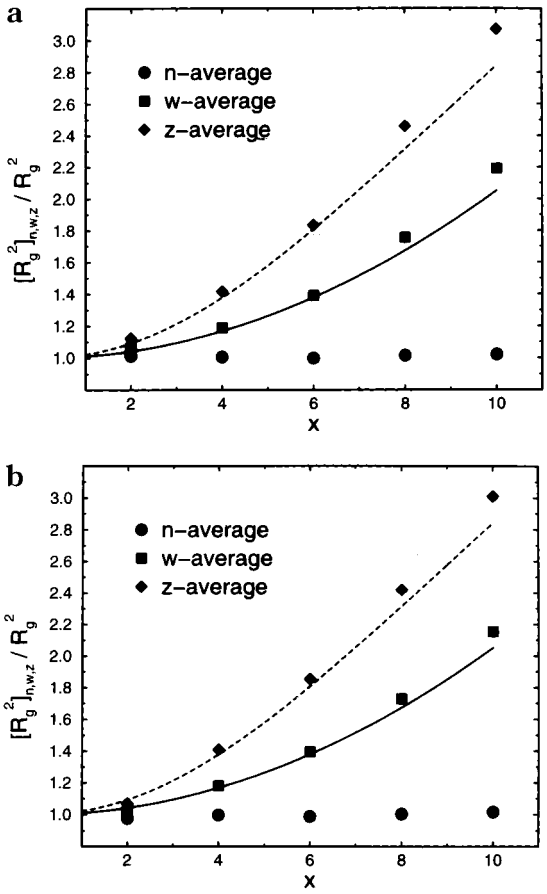

Figure 8. Counterpart to Figure 3 for the model mimicking polyethylene. The figure shows the number-, weight- and z-average radius of gyration, normalized by the monodisperse value, at $T = 380$ K ($R_g^2 \simeq 2.12$ nm^2) as a function of the polydispersity parameter x. Note that the number-average value is independent of x, whereas the dependence of the weight- and the z-average values closely follows the ideal behavior of eq 31.

Figure 7c additionally shows a solid line for the monodisperse data. It represents the results of a linear regression of the form $[R_g^2]_z^{1/2} = aT + b$ for the interval 380 K $\leq T \leq$ 470 K. This kind of analysis is motivated by a small-angle neutron scattering experiment studying the thermal expansion coefficient of the chains, $\kappa = \mathrm{d}(\ln R_{g,z}^2)/\mathrm{d}T$,[56] which was done on nearly monodisperse samples of long chains ($N_w \approx 2286, 3786$; $N_w/N_n < 1.05$). The fit yields $a \approx (-7.4 \pm 0.9) \times 10^{-4}$ nm/K and $b \approx (1.73 \pm 0.04)$ nm, and so $\kappa \approx (1.02 - 1.07) \times 10^{-3}$ K^{-1} in the studied temperature interval. A similar result is obtained when fitting the data for $x = 2$ ($N_w/N_n = 1.04$). This κ value agrees fairly well with the experimental result $\kappa_{exp} = 1.06 \times 10^{-3}$ K^{-1}.

Another closely related quantity is the characteristic ratio, $C_N = R^2/(N-1)\langle l^2\rangle$. Experimentally, this quantity is mostly determined by neutron scattering and is given by $C_N^{ns} = 6R_{g,z}^2/(N_w - 1)\langle l^2\rangle$. Figure 9 shows C_N^{ns} as a function of temperature for $1.04 \leq N_w/N_n \leq 2$. Due to the sensitivity of the weight- and the z-averages to large chain lengths, the small amount of long chains (20%) already leads to a considerable enhancement of C_N^{ns} with respect to the monodisperse result. This effect of polydispersity has to be borne in mind when comparing chemically realistic simulation results for monodisperse melts to experimental data. Considering the coarseness of our model, we consider the agreement between it and

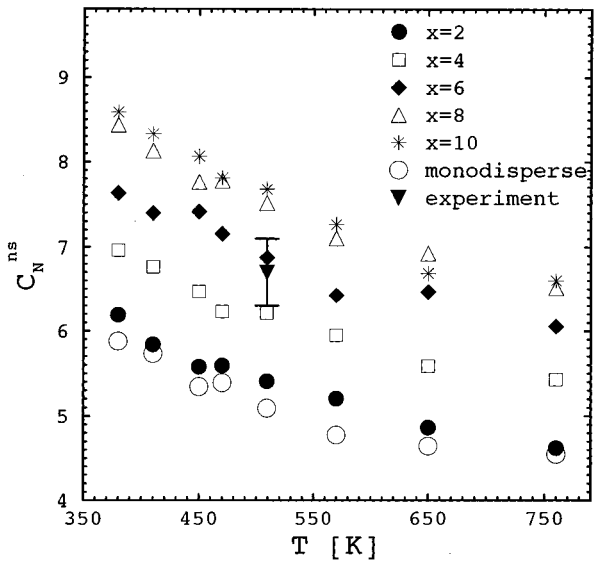

Figure 9. Characteristic ratio, defined as $C_N^{ns} = 6R_{g,z}^2/(N_w - 1)\langle l^2\rangle$, vs temperature for five different polydispersity parameters x. $R_{g,z}^2$ is the z-averaged radius of gyration and N_w the weight-averaged chain length. This definition agrees with the results obtained from scattering experiments. All simulation results are for the bond-fluctuation model with potentials adapted to polyethylene. The x-values correspond to $N_w/N_n = 1.04$ ($x = 2$), $N_w/N_n = 1.16$ ($x = 4$), $N_w/N_n = 1.36$ ($x = 6$), $N_w/N_n = 1.64$ ($x = 8$), and $N_w/N_n = 2$ ($x = 10$). In addition, the monodisperse result ($N = 20$) and an experimental value, $C_N^{exp} \simeq 6.7 \pm 0.4$, at $T = 509$ K are shown. The experimental data point was estimated from the C_∞ value ($C_\infty \simeq 7.8 \pm 0.4$ at $T = 413$ K) of small-angle neutron scattering experiments[59] on nearly monodisperse polyethylene melts ($N_w/N_n = 1.05$) in ref 60.

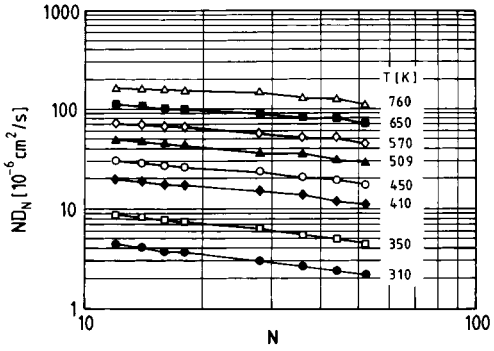

Figure 10. Self-diffusion coefficient, D_N, multiplied by the chain length, N, in a log−log plot vs N for different temperatures, as indicated. The simulation results are for the bond-fluctuation model with potentials adapted to polyethylene. The coarse-grained chain length, N, correponds to the degree of polymerization, $N_p = 5N$, for polyethylene.

the experimental value (obtained by RIS extrapolation[60] from the value in ref 59), shown with the error bar in Figure 9, to be satisfactory.

We now turn to the dynamic properties of our model. Figure 10 shows the chain length dependence of the diffusion coefficient for various temperatures. It is the thermal counterpart to Figure 4a. As at $T = \infty$, the diffusion constant does not exhibit pure Rouse behavior, $D_N \sim 1/N$, but has a larger N-dependence. This deviation becomes more pronounced with decreasing temperature. The motion of long chains slows down more strongly than that of short chains. A possible explanation is motivated by the glassy behavior of monodisperse melts. In monodisperse melts there is a systematic

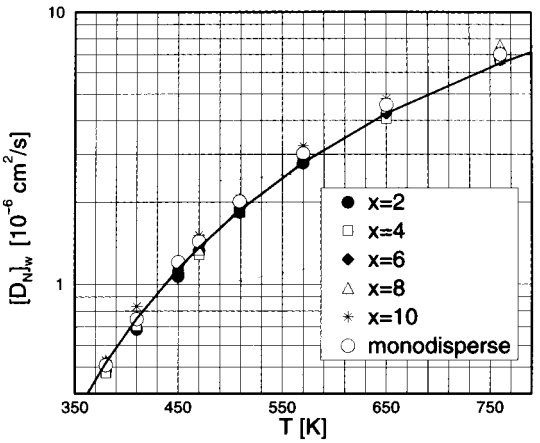

Figure 11. Weight-averaged diffusion coefficient, $[D_N]_w$, vs temperature for five different polydispersities: $N_w/N_n = 1.04$ ($x = 2$), $N_w/N_n = 1.16$ ($x = 4$), $N_w/N_n = 1.36$ ($x = 6$), $N_w/N_n = 1.64$ ($x = 8$), and $N_w/N_n = 2$ ($x = 10$). In addition, the monodisperse result ($N = 20$) is shown as open circles, and the fit result (solid line) to an Arrhenius equation is included (see text for parameters). The fit was done with the monodisperse data in the temperature interval 210 K ≤ T ≤ 760 K.

dependence of the glass transition temperature, T_g, on chain length, $T_g(N) = T_g(\infty)(1 - \text{const}/N)$. Thus it is plausible that a reduction of temperature has a larger effect on longer chains, in qualitative accord with Figure 10. A more quantitative understanding of the data is, however, hard to obtain.

On the other hand, the deviation from Rouse-like behavior in the studied temperature range is not so pronounced that the predictions of section III are violated. Figure 11 shows that the weight-averaged diffusion coefficient is nearly independent of polydispersity, in agreement with the results at infinite temperature (see Figure 5). Moreover, the simulation data for the bidisperse melts exhibit the same temperature dependence as the monodisperse system. A satisfactory description of the temperature dependence is obtained by an Arrhenius equation, $D(T) = D_\infty \exp[-E_A/T]$, with $D_\infty \approx 8.2 \times 10^{-5}$ cm^2/K and $E_A \approx 1923$ K. The latter value lies in the same range as the results of viscosity measurements by Pearson *et al.*,[46] who extracted an apparent activation energy, defined as the slope of an Arrhenius plot at $T = 423$ K, of $E_A = 2500-3000$ K for comparable molecular weight. This is only an apparent activation energy because Pearson *et al.* reanalyzed their data in terms of the friction coefficient and concluded that they were more compabtible with a Vogel−Fulcher behavior. The stronger temperature dependence compared to the simulation was already noticed in our previous work[23] and may be attributed to different ensembles used in the simulation (constant volume) and experiments (constant pressure).[61]

Figure 12 shows the results for the chain length dependence of the relaxation time τ_N. To facilitate the comparison with the athermal data of Figure 4b we give τ_N in MCS instead of in seconds (the conversion can be done by multiplying τ_N by eq 8). When one fits straight lines to the data of Figure 12, assuming $\tau_N \sim N^{z_{eff}}$, the effective exponent, $z_{eff}(T)$, increases from about 2.45 at high temperatures to about 2.8 at low temperatures (remember that the athermal value found for the same range of N was $z_{eff} \approx 2.37$; cf. Figure 4b). Should one interprete this finding as an evidence that the crossover toward a reptation-like behavior[8,52] sets in at low temperatures, even if N is not much larger than N_e? In

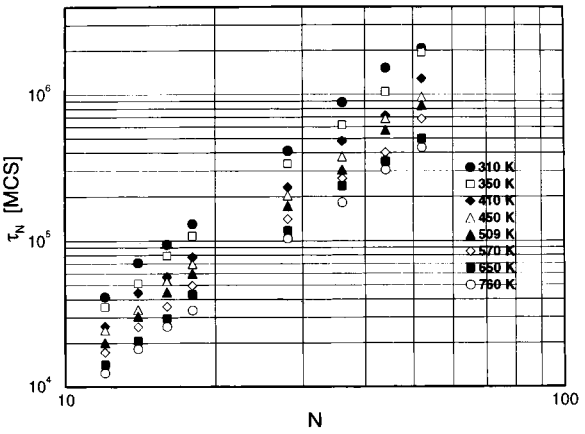

Figure 12. Log−log plot of the relaxation time, τ_N, vs chain length N for eight different temperatures as indicated. Note that τ_N is given in MCS's to allow a comparison with the athermal results of Figure 4b. The conversion to seconds can be done by multiplation with eq 8. The model is the same as in Figure 10.

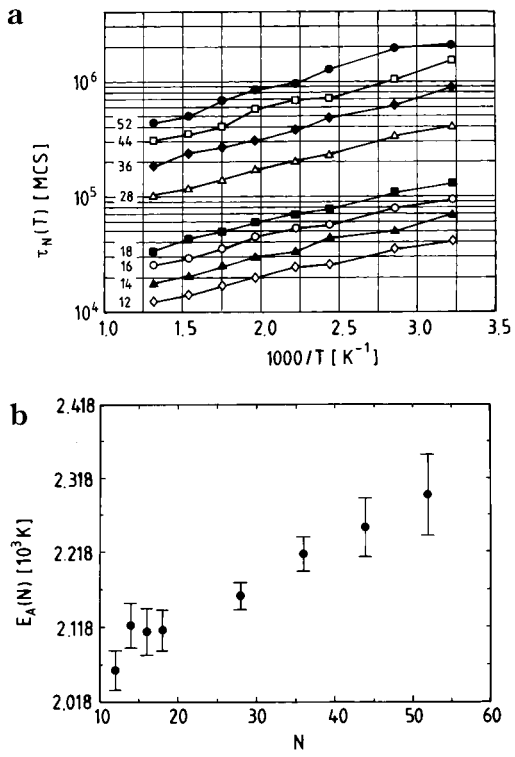

Figure 13. (a) Relaxation time, τ_N, plotted vs inverse temperature (temperature in units of K, while τ_N is in Monte Carlo steps [MCS]). Eight different chain lengths, N, are included, as indicated. These chain lengths correspond to a degree of polymerization of $N_p = 5N$. (b) Activation energy, $E_A(N)$ (in units of 10^3 K), plotted vs chain length, N, as obtained by fitting the formula $\tau_N(T) = \tau_N(\infty)\exp[E_A(N)/T]$. The model is the same as in Figure 10.

our opinion, one has to be very careful with such a conclusion, since alternative interpretations are equally well possible. For instance, Figure 13a shows τ_N plotted vs $1/T$ with N as a parameter. It is apparent that the data can be described by an Arrhenius equation with an activation energy, $E_A(N)$, that increases with N (see Figure 13b), *i.e.*, $\tau_N(T) = \tau_N(\infty)\exp[E_A(N)/T] \sim N^{2.37}\exp[E_A(N)/T]$. This could simply result from a chain end effect, $E_A(\infty) - E_A(N) \sim 1/N$. However, the limited range of N and the large error bars preclude any conclusion whether such a simple explanation is actually correct.

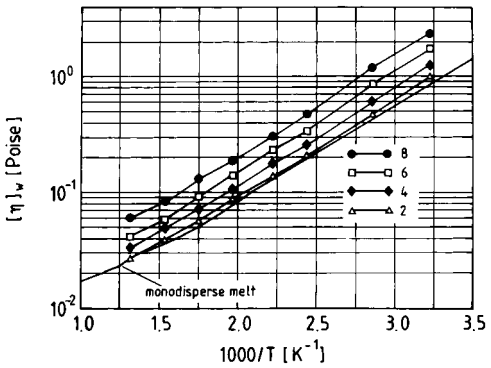

Figure 14. Weight-averaged viscosity, $[\eta]_w$, vs $1000/T$ for four different polydispersities: $N_w/N_n = 1.04$ ($x = 2$), $N_w/N_n = 1.16$ ($x = 4$), $N_w/N_n = 1.36$ ($x = 6$), and $N_w/N_n = 1.64$ ($x = 8$). The viscosity was calculated from the Rouse formula, eq 33. The solid line represents the monodisperse result. All data are are for the bond-fluctuation model with potentials adapted to polyethylene.

Therefore, even without invoking the development of anisotropic, reptation-like motion, one would expect long chains to relax more slowly and the difference between short and long chains to become more pronounced with decreasing temperature. This could also give rise to the observed increase of the N dependence at low temperatures.

Finally, Figure 14 presents the weight-average of the viscosity. The preceding discussion showed that the Rouse theory—though not strictly valid—provides a reasonable guideline for the interpretation of the simulation data. Therefore we determined the viscosity of the bidisperse polyethylene-like melts by the weight-average of the Rouse formula[8]

$$[\eta]_w = \frac{k_B T \phi}{288 s^3}\left[\frac{R^2}{N D_N}\right]_w \text{ [P]} \qquad (33)$$

For monodisperse melts, this equation yields a good description of experimental data.[23] The reason for calculating the weight-average is that this is the experimentally measured average because the viscosity depends on the size and thus on the weight of the polymer.[11] Figure 14 compares the monodisperse data with the results for $x = 2$, 4, 6, and 8. It shows that an increase of the polydispersity leads to an enhancement of the viscosity, but does not influence the temperature dependence. The curves are essentially shifted parallel to larger viscosities. Qualitatively, this behavior agrees with the predictions of the Schulz−Flory distribution, if N_n is kept constant while varying the polydispersity (as done in our simulation).[45] Quantitatively, however, the shift is bigger than expected from $[\eta]_w \sim N_w$ and eq 14. For instance, if $x = 8$, this would imply an enhancement of the viscosity beyond the monodisperse value by a factor of 1.64, whereas the actual increase is about twice as large. Nevertheless, the data qualitatively agree with the Rouse prediction $[\eta]_w[D_N]_w \sim N_w/N_n$ (see Figure 11). Since the product ηD_N is often used in the analysis of the crossover from Rouse to reptation dynamics, its sensitivity to the molecular weight distribution must be kept in mind when comparing different experiments, as also discussed in ref 46.

V. Concluding Remarks

The present paper summarizes our first attempts to model the influence of polydispersity on the static and

dynamic properties of polymer melts. The simulations were done with a coarse-grained lattice model, the bond-fluctuation model, for which monodisperse melts have been studied extensively.[3,37,38] This allows a comparison between the (average) behavior of a chain immersed in a environment of the same species with that of a chain surrounded by others of different length.

In the simulation polydispersity is realized in the simplest imaginable way by a bidisperse mixture of short and long chains. There are always 80% short and 20% long chains, and the chain length disparity is chosen such that the number-average chain length, N_n, is kept constant (see eq 14). Varying the polydispersity, N_w/N_n (between 1 and 2), therefore implies that the weight-average chain length, N_w, increases with polydispersity (see eq 14).

Simulations have been carried out for both athermal and thermal conditions. In the latter case the bond length and bond angle potentials are adjusted to mimic large length and time scale properties of polyethylene melts.[23]

Under athermal conditions, the end-to-end distance and the radius of gyration of the monodisperse and the bidisperse melts coincide (see Figure 1). This exemplifies that the change of environment does not perturb the static properties of the chains. They still retain their (almost) Gaussian structure typical of dense melts. Therefore the number-, weight-, and *z*-averaged radii of gyration agree very well with the expectations for ideal chains (see Figure 3). On the other hand, the dynamic properties are affected when introducing polydispersity. The presence of the (sluggish) long chains reduces the mobility and relaxation rate of the short species (see Figure 4). This influence is similar to the one observed in melts with randomly placed rigid obstacles.[57] A small amount of these obstacles leaves the static properties nearly unchanged but considerably slows down the motion of the chains. However, contrary to rigid obstacles, the long polymers in the present case are mobile and can also be influenced by the short chains. The short chains accelerate the long species so that the overall chain length dependence of the diffusion coefficient or the relaxation time is weaker than for monodisperse melts and thus closer to the Rouse prediction. Therefore the number-, weight-, and *z*-averaged diffusion coefficients agree reasonably well with the Rouse theory (see Figure 5), though the accord is certainly not as good as for the radii of gyration.

When the athermal model is extended by potentials adapted to simulate polyethylene, the just described effects of polydispersity are essentially retained (for instance, compare Figure 8 with Figure 3 or Figure 11 with Figure 5). The introduction of the potentials leads to a stiffening of the chains with decreasing temperature, which reflects the increase of bonds populating the trans-state in polyethylene. This stiffening reduces the number of statistical segments and makes the chains less ideal so that the deviations from the Gaussian predictions are more pronounced than in the athermal case (compare Figure 8 and Figure 3). Furthermore, the simulation results for experimentally accessible quantities, such as the characteristic ratio, C_N (see Figure 9), or the product of the diffusion coefficient and viscosity, ηD_N (Figures 11 and 14), point out that these quantities depend on polydispersity. This has to be kept in mind when quantitatively comparing simulational or theoretical results to experimental data.

Acknowledgment. We are grateful to the Bundesministerium für Bildung, Wissenschaft, Forschung und Technologie and to the Bayer Corporation for financial support under Grant No. 3M40708 and Grant No. 03N8008C.

References and Notes

(1) Bicerano, J., Ed. *Computational Modeling of Polymers*, Dekker: New York, 1992.
(2) Binder, K., Ed. *Monte Carlo and Molecular Dynamics Simulations in Polymer Science*, Oxford University Press: New York, 1995.
(3) Binder, K.; Paul, W. *J. Polym. Sci. Part B: Polym. Phys.* **1997**, *35*, 1.
(4) Roe, R. J., Ed. *Computer Simulation of Polymers*; Prentice-Hall: Englewood Cliffs, NJ, 1991.
(5) Li, B.; Madras, N.; Sokal, A. D. *J. Stat. Phys.* **1995**, *80*, 661.
(6) Sokal, A. D. In *Monte Carlo and Molecular Dynamics Simulations in Polymer Science*; Binder, K., Ed.; Oxford University Press: New York, 1995.
(7) Paul, W.; Yoon, Do Y.; Smith, G. D. *J. Chem. Phys.* **1995**, *103*, 1702. Smith, G. D.; Paul, W.; Yoon, Do Y.; Zirkel, A.; Hendricks, J.; Richter, D.; Schober, H. *Local Dynamics in a Long-chain Alkane Melt from Molecular Dynamics Simulations and Neutron Scattering Experiments*, *J. Chem. Phys.* **1997**, *107*, 4751.
(8) Doi, M.; Edwards, S. F. *The Theory of Polymer Dynamics*; Clarendon Press: Oxford, England, 1986.
(9) Elias, H. G. *Makromoleküle: Struktur-Eigenschaften-Synthesen-Stoffe-Technologie*, Hüthig and Wepf: Basel, Switzerland, 1981; Chapter 8.
(10) Strobl, G. R. *The Physics of Polymers: Concepts for Understanding their Structures and Behavior*; Springer: Berlin, 1996.
(11) Flory, P. J. *Principles of Polymer Chemistry*, Cornell University Press: Ithaca, NY, 1953.
(12) Clarke, J. H. R.; Brown, D. *Mol. Phys.* **1986**, *58*, 815; **1987**, *3*, 27.
(13) Rigby, D.; Roe, R. J. *J. Chem. Phys.* **1987**, *87*, 7285; **1988**, *89*, 5280; *Macromolecules* **1989**, *22*, 2259.
(14) Toxvaerd, S. *J. Chem. Phys.* **1990**, *93*, 4290. Padilla, P.; Toxvaerd, S. *Ibid*. **1991**, *94*, 5650.
(15) Karasawa, N.; Dasgupta, S.; Goddard, W. A. *J. Phys. Chem.* **1991**, *95*, 2260.
(16) Tackeuchi, H.; Roe, R. J. *J. Chem. Phys.* **1991**, *94*, 7446.
(17) Baschnagel, J.; Binder, K.; Paul, W.; Laso, M.; Suter, U. W.; Batoulis, I.; Jilge, W.; Bürger, T. *J. Chem. Phys.* **1991**, *95*, 6014.
(18) Baschnagel, J.; Qin, K.; Paul., W.; Binder, K. *Macromolecules* **1992**, *25*, 3117.
(19) Pant, P. V. K.; Han, J.; Smith, G. D.; Boyd, R. H. *Macromolecules* **1992**, *25*, 200. Pant, P. V. K.; Boyd, R. H. *Macromolecules* **1992**, *25*, 494.
(20) Siepmann, J. I.; Kanaborni, S.; Smit, B. *Nature* **1993**, *365*, 330.
(21) Yoon, Do Y.; Smith, G. D.; Matsuda, T. J. *J. Chem. Phys.* **1993**, *98*, 10037. Smith, G. D.; Yoon, Do Y. *J. Chem. Phys.* **1994**, *100*, 649. Smith, G. D.; Yoon, Do Y.; Zhu, W.; Ediger, M. *Macromolecules* **1994**, *27*, 5563.
(22) Brown, D.; Clarke, J. H. R.; Okuda, M.; Yamazaki, T. *J. Chem. Phys.* **1994**, *100*, 1684; *Comput. Phys. Commun.* **1994**, *83*, 1.
(23) Tries, V.; Paul, W.; Baschnagel, J.; Binder, K. *J. Chem. Phys.* **1997**, *106*, 738.
(24) Vacatello, M. *Macromol. Theory Simul.* **1997**, *6*, 613.
(25) Kremer, K.; Binder, K. *Comp. Phys. Rep.* **1988**, *7*, 259.
(26) Joanny, J.-F. *C. R. Acad. Sci., Ser. B* **1978**, *286*, 89.
(27) Koningsveld, R.; Chermin, R. A. G.; Gordon, M. *Proc. R. Soc. London, A* **1970**, *319*, 331. Koningsveld, R.; Kleintjens, L. A. *Macromolecular Chemistry*; Butterworths: London, 1973; Vol. 1, p 97.
(28) Schichtel, T. E.; Binder, K. *Macromolecules* **1987**, *20*, 1671.
(29) Cherayil, B. J.; Kholodenko, A. L.; Freed, K. F. *J. Chem. Phys.* **1987**, *86*, 7204.
(30) Hertanto, A.; Dickman, R. *J. Chem. Phys.* **1990**, *93*, 774.
(31) Doi, M.; Graessley, W. W.; Helfand, E.; Pearson, D. S. *Macromolecules* **1987**, *20*, 1900.
(32) Viovy, J. L.; Rubinstein, M.; Colby, R. H. *Macromolecules* **1991**, *24*, 3587.
(33) Wilson, J. D.; Loring, R. F. *J. Chem. Phys.* **1995**, *103*, 1641.

(34) Rathgeber, S; Zirkel, A.; Willner, L.; Richter, D.; Brulet, A.; Farago, B. *Physica B* **1997**, *234−236*, 258.
(35) Carmesin, I.; Kremer, K. *Macromolecules* **1988**, *21*, 2819.
(36) Deutsch, H.-P.; Binder, K. *J. Chem. Phys.* **1991**, *94*, 2249.
(37) Paul, W.; Binder, K.; Heermann, D. W.; Kremer, K. *J. Phys. (Paris) II* **1991**, *1*, 37.
(38) Paul, W.; Binder, K.; Heermann, D. W.; Kremer, K. *J. Chem. Phys.* **1991**, *95*, 7726.
(39) Rouse, P. E. *J. Chem. Phys.* **1953**, *21*, 127.
(40) Tries, V. Dissertation; Johannes-Gutenberg Universität: Mainz, Germany, 1996 (unpublished).
(41) Paul, W.; Pistoor, N. *Macromolecules* **1994**, *27*, 1249.
(42) Greschner, G. S. *Makromol. Chem.* **1973**, *170*, 203.
(43) Appelt, B.; Meyerhoff, G. *Macromolecules* **1980**, *13*, 657.
(44) Odian, G. *Principles of Polymerization*; Wiley: New York, 1981.
(45) Kamide, K.; Saito, M. In *Determination of Molecular Weight*; *Chemical Analysis*, Cooper, A. D., Ed.; Wiley: New York, 1989; Vol. 133.
(46) Pearson, D. S.; Fetters, L. J.; Graessley, W. W.; Ver Srate, G.; von Meerwall, E. *Macromolecules* **1994**, *27*, 711. Pearson, D. S.; Ver Srate, G.; von Meerwall, E.; Schilling, F. C. *Macromolecules* **1987**, *20*, 1133.
(47) Ewen, B.; Richter, D. *Adv. Polym. Sci.* **1997**, *134*, 1.
(48) Dünweg, B.; Stevens, M.; Kremer, K. In *Monte Carlo and Molecular Dynamics Simulations in Polymer Science*; Binder, K., Ed.; Oxford University Press: New York, 1995; p 125.
(49) Higgins, J. S.; Benoit, H. C. *Polymers and Neutron Scattering*; Clarendon: Oxford, England, 1994.
(50) Verdier, P. H. *J. Chem. Phys.* **1966**, *45*, 2118.
(51) Joanny, J. F.; Grant, P.; Turkevich, L. A.; Pincus, P. *J. Phys.* **1981**, *42*, 1045. Joanny, J. F.; Grant, P.; Pincus, P.; Turkevich, L. A. *J. Appl. Phys.* **1981**, *52*, 5943.
(52) de Gennes, P.-G. *Scaling Concepts in Polymer Physics*; Cornell University Press: Ithaca, NY, 1979.
(53) Flory, P. J. *Statistical Mechanics of Chain Molecules*; Carl Hanser Verlag: München, Germany, 1989.
(54) Baschnagel, J.; Binder, K.; Milchev, A. *Mobility of Polymers Near Surfaces*. In *Polymer Surfaces, Interfaces and Thin Films*; Karim, A.; Kumar, S., Eds.; World Scientific: Singapore, in press.
(55) Kopf, A.; Dünweg, B.; Paul, W. *J. Chem. Phys.* **1997**, *107*, 6945.
(56) Boothroyd, A. T.; Rennie, A. R.; Boothroyd, C. B. *Europhys. Lett.* **1991**, *15*, 715.
(57) Gerroff, I.; Milchev, A.; Binder, K.; Paul, W. *J. Chem. Phys.* **1993**, *98*, 6526.
(58) Wittmer, J. Diplomarbeit; Johannes-Gutenberg Universität: Mainz, 1991 (unpublished).
(59) Horton, J. C.; Squires, G. L.; Boothroyd, A. T.; Fetters, L. J.; Rennie, R. J.; Glinka, C. J.; Robinson, R. A. *Macromolecules* **1989**, *22*, 681.
(60) Paul, W.; Yoon, Do Y.; Smith, G. D. *Macromolecules* **1997**, *30*, 7772.
(61) Bennemann, C.; Paul, W.; Binder, K.; Dünweg, B. *Phys. Rev. E* **1997**, *57*, 843.

MA9718863